



Swansea University
Prifysgol Abertawe



Cronfa - Swansea University Open Access Repository

This is an author produced version of a paper published in :
Applied Physics Letters

Cronfa URL for this paper:
<http://cronfa.swan.ac.uk/Record/cronfa32459>

Paper:

Sedghi, N., Li, H., Brunell, I., Dawson, K., Potter, R., Guo, Y., Gibbon, J., Dhanak, V., Zhang, W., Zhang, J., Robertson, J., Hall, S. & Chalker, P. (2017). The role of nitrogen doping in ALD Ta₂O₅ and its influence on multilevel cell switching in RRAM. *Applied Physics Letters*, 110(10), 102902
<http://dx.doi.org/10.1063/1.4978033>

This article is brought to you by Swansea University. Any person downloading material is agreeing to abide by the terms of the repository licence. Authors are personally responsible for adhering to publisher restrictions or conditions. When uploading content they are required to comply with their publisher agreement and the SHERPA RoMEO database to judge whether or not it is copyright safe to add this version of the paper to this repository.

<http://www.swansea.ac.uk/iss/researchsupport/cronfa-support/>

The role of nitrogen doping in ALD Ta₂O₅ and its influence on multilevel cell switching in RRAM

N. Sedghi, H. Li, I. F. Brunell, K. Dawson, R. J. Potter, Y. Guo, J. T. Gibbon, V. R. Dhanak, W. D. Zhang, J. F. Zhang, J. Robertson, S. Hall, and P. R. Chalker

Citation: *Appl. Phys. Lett.* **110**, 102902 (2017); doi: 10.1063/1.4978033

View online: <http://dx.doi.org/10.1063/1.4978033>

View Table of Contents: <http://aip.scitation.org/toc/apl/110/10>

Published by the [American Institute of Physics](#)

Articles you may be interested in

[Oxygen migration during resistance switching and failure of hafnium oxide memristors](#)
Appl. Phys. Lett. **110**, 103503103503 (2017); 10.1063/1.4974535

[The effect of oxygen vacancy on switching mechanism of ZnO resistive switching memory](#)
Appl. Phys. Lett. **110**, 073501073501 (2017); 10.1063/1.4976512

[A niobium oxide-tantalum oxide selector-memristor self-aligned nanostack](#)
Appl. Phys. Lett. **110**, 103102103102 (2017); 10.1063/1.4977945

[Temperature and field-dependent transport measurements in continuously tunable tantalum oxide memristors expose the dominant state variable](#)
Appl. Phys. Lett. **110**, 123501123501 (2017); 10.1063/1.4978757

[A cell-based clustering model for the reset statistics in RRAM](#)
Appl. Phys. Lett. **110**, 123503123503 (2017); 10.1063/1.4978756

[Current-induced surface roughness reduction in conducting thin films](#)
Appl. Phys. Lett. **110**, 103103103103 (2017); 10.1063/1.4977024

Fearful for the future of science?

Sign up for **FREE** FYI emails.
AIP American Institute of Physics

The role of nitrogen doping in ALD Ta₂O₅ and its influence on multilevel cell switching in RRAM

N. Sedghi,^{1,a)} H. Li,² I. F. Brunell,³ K. Dawson,³ R. J. Potter,³ Y. Guo,^{2,4} J. T. Gibbon,⁵ V. R. Dhanak,⁵ W. D. Zhang,⁶ J. F. Zhang,⁶ J. Robertson,² S. Hall,¹ and P. R. Chalker³

¹Department of Electrical Engineering and Electronics, University of Liverpool, Liverpool L69 3GJ, United Kingdom

²Department of Engineering, University of Cambridge, Cambridge CB2 1TN, United Kingdom

³School of Engineering, University of Liverpool, Liverpool L69 3GH, United Kingdom

⁴College of Engineering, Swansea University, Swansea SA1 8EN, United Kingdom

⁵Department of Physics, University of Liverpool, Liverpool L69 7ZE, United Kingdom

⁶Department of Electronics and Electrical Engineering, Liverpool John Moores University, Liverpool L3 3AF, United Kingdom

(Received 6 December 2016; accepted 22 February 2017; published online 6 March 2017)

The role of nitrogen doping on the stability and memory window of resistive state switching in N-doped Ta₂O₅ deposited by atomic layer deposition is elucidated. Nitrogen incorporation increases the stability of resistive memory states which is attributed to neutralization of electronic defect levels associated with oxygen vacancies. The density functional simulations with the screened exchange hybrid functional approximation show that the incorporation of nitrogen dopant atoms in the oxide network removes the O vacancy midgap defect states, thus nullifying excess defects and eliminating alternative conductive paths. By effectively reducing the density of vacancy-induced defect states through N doping, 3-bit multilevel cell switching is demonstrated, consisting of eight distinctive resistive memory states achieved by either controlling the set current compliance or the maximum voltage during reset. Nitrogen doping has a threefold effect: widening the switching memory window to accommodate the more intermediate states, improving the stability of states, and providing a gradual reset for multi-level cell switching during reset. The N-doped Ta₂O₅ devices have relatively small set and reset voltages (< 1 V) with reduced variability due to doping. *Published by AIP Publishing.* [<http://dx.doi.org/10.1063/1.4978033>]

Resistive-switching random access memory (RRAM) is the focus of development as a substitute for existing non-volatile memory (NVM) devices. In metal oxide based RRAM devices, switching between low resistive and high resistive states (LRS and HRS, respectively) occurs by field-assisted diffusion of defects such as oxygen vacancies (O_{vac}) to form a conductive “filament” (CF).¹ By applying appropriate voltages across the oxide, the CF can be formed, ruptured, and restored to switch between the “on” and “off” memory states. It is crucial to engineer the oxygen vacancy profile in the oxide film to achieve stable memory states and a large switching memory window for immunity to noise.² Extending this requirement further leads to the prevention of multiple potential CFs with different LRS resistances, which is the main cause of the variability in the multilevel cell (MLC) switching states.³ The MLC switching enables multi-bit storage capacity and potentially increases the storage capacity for ultra-high density memory applications. It has been reported that the variability of resistance associated with a CF depends on the conductive filament size and also on the oxygen vacancy concentration.^{4–6} The multilevel switching is commonly achieved by adjusting the LRS resistance by setting the current compliance during the set cycle.^{3,4,7,8} Less common is to change the HRS current by changing the maximum voltage during the reset (V_{\max}).^{8,9} The latter suffers from

larger HRS resistance variability since that depends mostly on the length of the ruptured part of the filament which varies from cycle to cycle. In the former method, the LRS resistance depends on the radius and conductivity of the filament, resulting in a far smaller variability. Therefore, MLC switching by the set current is mostly used and 3-bit cells using this method have been reported.^{3,7} However, the low resistance states at small set currents, within the lower region of memory window, have poor stability and the device often fails to be set or reset. Here, we have combined the two MLC switching methods using N-doped atomic layer deposited (ALD) Ta₂O₅ based RRAM devices. This approach facilitates the achievement of more than 3-bit MLC by varying the low resistance states in the upper half of the memory window by set current compliance and high resistance states in the lower part by V_{\max} . The role of N doping is to control the oxygen density in the film, first to widen the memory window to accommodate more intermediate states, second, to improve the stability of states, and third, to extend the region of gradual reset to lower currents, which is essential for MLC switching of HRS resistance.

The selection of an appropriate switching layer material is central to the RRAM operation,¹⁰ and tantalum oxide is of particular interest because of its high endurance of switching cycles.¹¹ The purpose of N doping is to reduce electronic defect states associated with the O_{vac}¹² and enabling the CFs to be formed with more stable and discrete resistances suitable for MLC switching. The improved state stability is believed to be due to the elimination of excess conducting

^{a)}Author to whom correspondence should be addressed. Electronic mail: nsed@liverpool.ac.uk.

paths in the oxide by passivation of oxygen vacancies by nitrogen atoms.³ Metal-insulator-metal (MIM) structures were fabricated on Corning glass or silicon wafer substrates. The bottom electrode is 50 nm Pt, with a 10 nm Cr adhesion layer, deposited by dc magnetron sputtering. The oxide layer, 15 nm thick Ta₂O₅ or N-doped Ta₂O₅, was deposited by conventional ALD, using the precursor Ta(OC₂H₅)₅ and H₂O as an oxidant. N doping was achieved by substituting a proportion of the water cycles with an aqueous NH₄OH solution, in the increasing ratios of 1:99, and 1:32, 1:11. The top electrode of 30 nm Ti, with a 60 nm Pt capping layer, was deposited by rf sputtering. Conventional photolithography and metal lift-off were used to define the top and bottom contacts and active device area of 512 overlapping and 512 cross-line square devices, with dimensions of 2 to 150 μm . The samples were annealed in forming gas ambient at 350° C for 1 h. This facilitated the electroforming and device switching, presumably by increasing the O vacancies reservoir at the top metal-oxide interface. A bright field transmission electron microscopy (BF-TEM) micrograph of the MIM structure is shown in Fig. 1. The inset diffraction patterns show that the tantalum oxide film remains amorphous even after the forming gas annealing. The dc set-reset cycles were performed by the return sweeps of a dc voltage from 0 V to a positive value, applied to the Ti contact, for the set and to a negative value for reset. The measurements were taken using either HP 4155 A or Agilent B1500 A Semiconductor Parameter Analyzers. The LRS resistance was programmed by setting the current compliance during the set cycle, and the HRS resistance was programmed by setting V_{max} . The resistance at each state was calculated at a “read” voltage of -0.1 V. The statistical variability of each programmed state was analyzed after performing 30 alternate set and reset cycles and calculating the cumulative distribution function (CDF) of resistance at each state. The same method was used to analyze the device to device variability on 25 devices in different regions of the sample.

Figure 2(a) shows the set and reset cycles of the devices made of undoped and N-doped Ta₂O₅ with various doping cycles, at a set current compliance of 1 mA. Electroforming

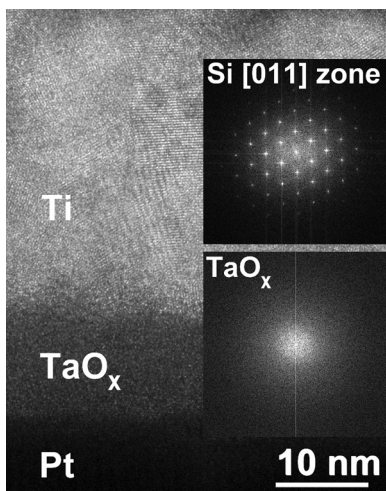


FIG. 1. BF-TEM image of device cross section and diffraction patterns from the TaO_x film and silicon substrate.

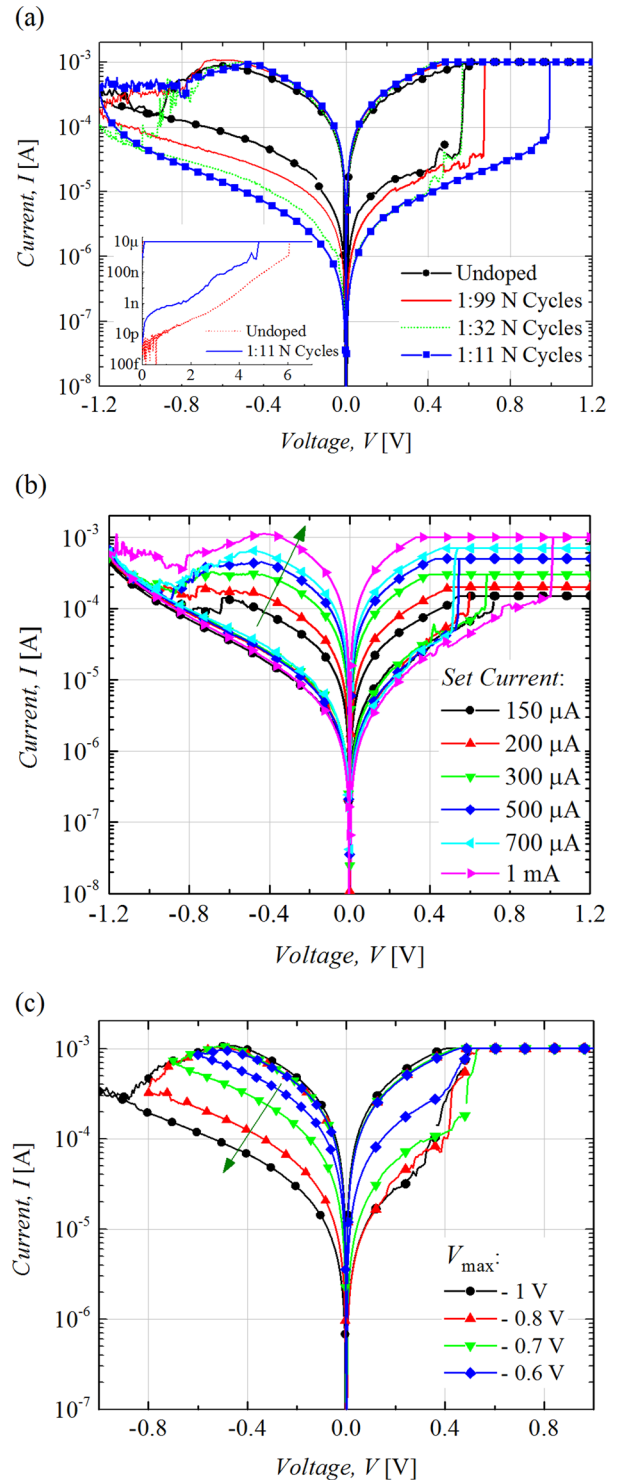


FIG. 2. (a) The switching characteristics of the N-doped and undoped RRAM devices at set current compliance of 1 mA. The forming IV characteristics are shown as an inset. Variation of LRS current with set current compliance (b) and HRS with V_{max} (c). The arrows show the direction of change in current with setting parameters.

was performed prior to the first reset cycle by a positive sweep up to 10 V to the Ti contact and current compliance of 10 μA , as shown in the inset of Fig. 2(a). The forming voltage was typically 6–8 V and no specific difference in forming voltage or its current-voltage shape was observed between the doped and undoped devices. The switching characteristics are independent of device area (4–22500 μm^2), which is in agreement

with previous reports¹¹ and indicates the presence of only one dominant conductive filament at a time in a given device. The memory window is significantly increased by the level of N doping, from 17 to 141 at -0.1 V for the 1:11 N doping cycles, due to the reduction in the HRS current in the N-doped device, which is attributed to a more resistive or longer ruptured region of conductive filament. For all of the doping cycle treatments used, the nitrogen incorporation in the films is at the detection limit of XPS measurements (not shown), implying that the N content is less than 2%. The sample with 1:12 N cycles has been used as an optimum choice for this study. The excess amount of N doping increases the resistance nonlinearity and variability.³ The variation in the LRS current with N doping is insignificant. The HRS current, however, is controlled by the ruptured region in the conductive filament. The decreased HRS current in N-doped devices can be attributed to a longer ruptured region of the filament and larger hopping distance due to a lower concentration of O vacancies.

The effect of set current compliance and V_{\max} on 1:12 N-doped devices is shown in Figs. 2(b) and 2(c), respectively. Varying the former, changes the LRS current and varying the latter changes the HRS current, both resulting in intermediate states within the upper and lower parts of the memory window, respectively, applicable for MLC switching. The increase in the LRS current with the increase in set current compliance is related to a larger radius of the conductive filament and also the higher concentration of O vacancies within the filament.⁴ The reduction in the HRS current with V_{\max} is due to a larger emigration rate of oxygen vacancies from the conductive filament, resulting in a longer ruptured region.

For MLC switching with a large number of intermediate states (3-bit or more), the device not only requires a large memory window to accommodate the states but also the states need to have small variability to prevent intermixing. It has been shown in the literature^{4,7} and in this work, that atomic doping can improve both requirements. Two types of variability in RRAM devices can be discussed, which, although related, are of a different nature. One is variability in resistance of a state during the successive set and reset cycles, which depends on the rupture and restoration of a particular filament in the device. The other is the device to device variability which depends on the uniformity of O vacancies within the film across the sample. Figure 3(a) shows the cumulative distribution function (CDF) of the resistance at 8 various states (3 bits) of the N-doped device programmed by set current compliance, read at the voltage of -0.1 V. The devices show good stability in LRS resistance with a large gap between highest LRS and lowest HRS resistances. The same graph for an undoped device is shown in Fig. 3(b) for comparison. Both N-doped and undoped devices have good stability at LRS; however, the undoped device shows more variability at low set currents and has significantly greater variability in HRS with a much smaller memory window. The device to device variability of the sample is also shown in the CDF plots of Fig. 3(c) for 25 devices with differing areas and locations across the sample. These data demonstrate the excellent stability at LRS, but the HRS resistance has a fairly large variability. The HRS variability is ascribed to variation in diameter of the critical filament region which affects the length of the ruptured part of a filament and hence the HRS

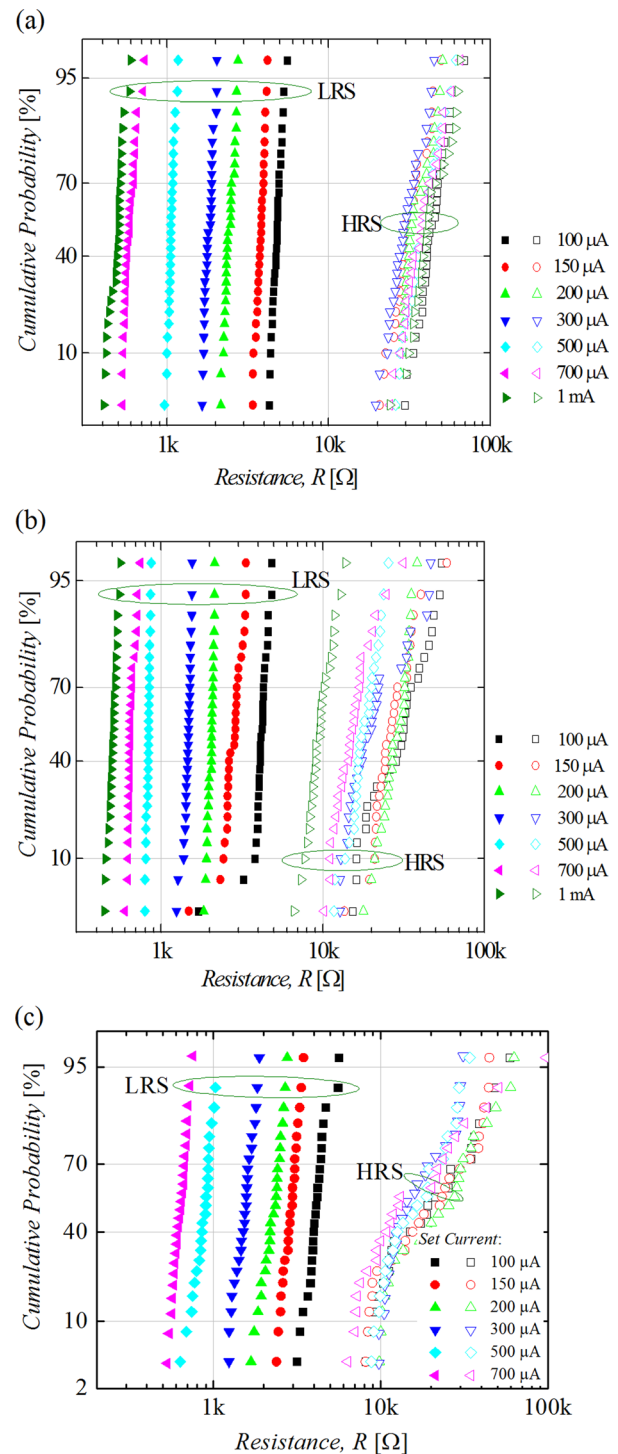


FIG. 3. The cumulative distribution of resistance states for N-doped (a) and undoped (b) devices. (c) The device to device distribution for 25 N-doped devices.

resistance. Evolution of a conductive filament and its rupture and restoration have been studied by a number of analytical and numerical models^{13–16} which have shed light on the device switching characteristics and the stability of states. The filament rupture and, hence, the HRS resistance after reset depends on the electric field distribution in the filament, and in particular, in the critical filament region; the narrowest part of the filament or the neck of its commonly described hourglass shape. The diameter of a filament in the critical region depends on the initial distribution of O vacancies

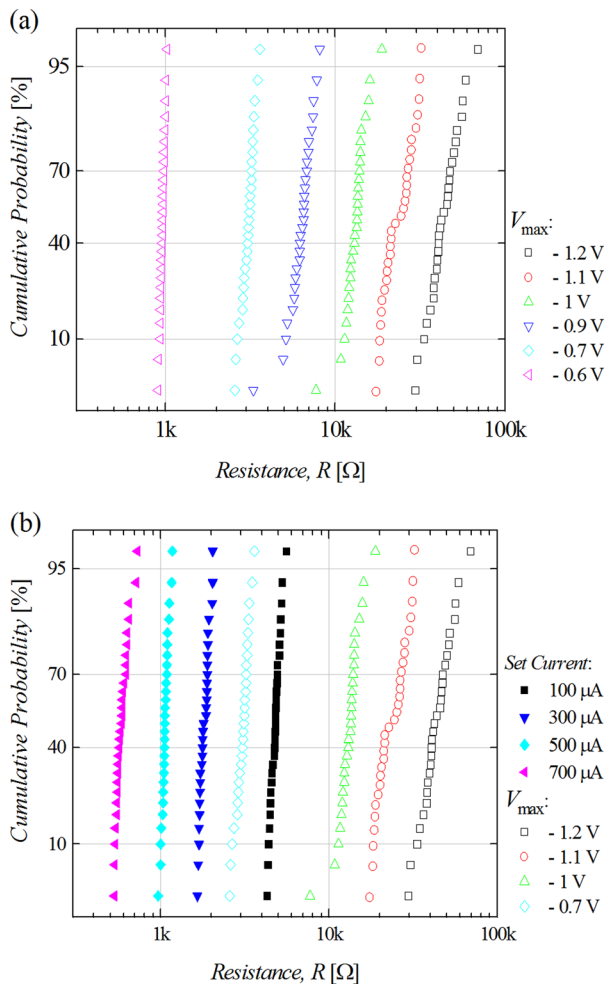


FIG. 4. (a) MLC switching by changing the HRS resistance by varying V_{max} . (b) Combination of two methods for 3-bit MLC. The solid and open symbols show LRS and HRS resistances, respectively.

within the film and their migration by the electric field. When it is narrow, the electric field in this region is stronger and more O vacancies are emigrated, resulting in a larger HRS resistance. Local Joule heating due to the LRS current before reset can also make the diameter larger.^{13,14}

The MLC by the set current is preferable because of good variability performance of the LRS resistance. Fig. 3(a) shows 3-bit MLC using only this method where the lower part of memory window remains unused. At very low set currents, the devices fail to switch (set and reset), and even if they do, the stability is very poor. This gap can be filled with high resistive states by changing V_{max} . Figure 4(a) shows the MLC with 6 states using this method. Combining the two MLC methods can provide 3-bit (8 states) or more, with large separation of states, as is shown in Fig. 4(b). By this method and with further improvement in device stability, 4-bit MLC is feasible, but this is unlikely to be achieved by setting either current or voltage individually.

We have previously reported the properties of O_{vac} in the λ phase of Ta_2O_5 crystal¹⁷ and the amorphous Ta_2O_5 network¹⁸ through sX density functional simulations. It is found that the 2-fold O_{vac} in both networks has a small formation energy, low diffusion barrier, and deep defect states below the conduction band, believed to be strongly related to the resistive switching behavior of the RRAM devices. Here, we have applied the sX hybrid functional density functional simulation to calculate the effect of N doping in the amorphous Ta_2O_5 network. The simulation settings are the same as in our previous work.¹⁸ The atomic structure and density of states (DOS) of the amorphous Ta_2O_5 network with a 2-fold O_{vac} are shown in Figs. 5(a) and 5(b), respectively. The O_{vac} gives rise to a deep defect state in the mid bandgap region, with the defect orbital localized on one nearby Ta atom. The effect of N doping has been studied by

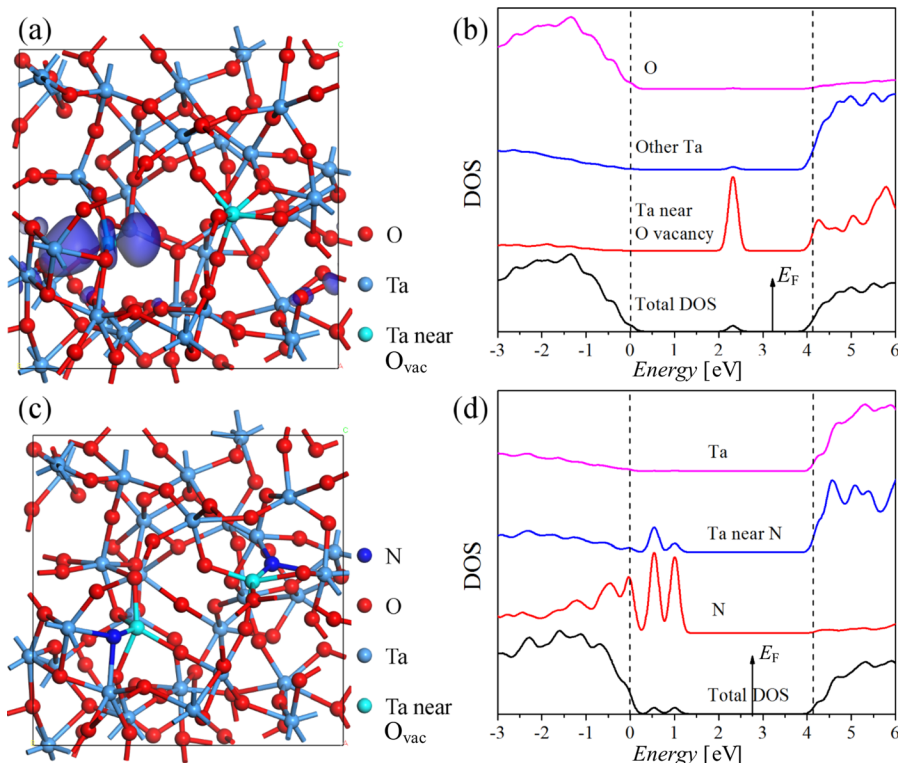


FIG. 5. (a) The atomic model and (b) the density of states of undoped amorphous Ta_2O_5 structure with an O vacancy. The blue isosurface shows defect orbital in mid bandgap. (c) The atomic model and (d) the density of states of amorphous Ta_2O_5 structure with two N atoms substituting two O atoms near the O vacancy site. The red, light blue, cyan, and dark blue balls denote O, Ta, Ta near O_{vac} , and N atoms, respectively.

substituting two O atoms with N atoms near the O_{vac} site, as shown in Fig. 5(c). The original O_{vac} defect state in the bandgap is removed as a result of N doping,¹² leaving some N non-bonding states near the valence band of Ta_2O_5 (Fig. 5(d)), as in the previous work.¹⁹

We now consider the mechanism that influences the HRS current and increases the resistance window between states due to the N doping process. The original O_{vac} introduces two excess electrons localized on the nearby Ta atom. During the doping process, each N atom substitutes one O atom in the network and creates a valence band hole. The two excess electrons from O_{vac} transfer to two nearby N atoms to fill their valence states and form a closed shell electronic configuration. Locally, the O_{vac} becomes a V^{2+} center, involving a certain lattice distortion, and pushes the original defect state up into the conduction band.¹² The energy gain of this process comes from the two electrons falling from mid gap states into the valence band holes, which compensates the energy required for local distortion. In this way, the 2-fold O_{vac} in the amorphous Ta_2O_5 network is nullified or cancelled by the presence of two N atoms. The neutralization of the defect states associated with the O_{vac} eliminates the excess conductive paths⁷ and reduces the numbers or densities of the potential filaments. This effect has been observed in sputtered TaO_x films by controlling the oxygen partial pressure during sputtering.⁴ It was concluded that the variability of the conductive filament resistance depends on both the filament diameter and the oxygen vacancy density in the filament. The model presented here shows that the effect of adding nitrogen to the ALD tantalum oxide can help to improve these factors and that multilevel switching is achievable in the N-doped film. It reduces the variability in the LRS current by preventing the set operation of the device through a different conductive path. It also makes the filament denser which decreases the HRS current due to a larger gap in the ruptured filament at critical filament region.

In conclusion, RRAM devices were fabricated by ALD Ta_2O_5 doped with nitrogen. The dc sweep set-reset measurements show that passivation of O_{vac} increases the switching memory window and the state's stability. The stability of states and the separation of states at various set currents enable the device for MLC switching applications.

The devices have set and reset voltages of less than 1 V and their variability is improved by doping. Density functional simulation of the atomic structures and calculation of density of states using sX hybrid functional correction show that N dopants substitute O atoms near the O_{vac} , resulting in nullifying the associated electronic defect states in the mid bandgap of the oxide, and thus eliminates the alternative conductive paths.

The work has been funded by the Engineering and Physical Sciences Research Council (EPSRC) UK, project numbers EP/M00662X/1, EP/M009297/1, and EP/M006727/1.

- ¹H. Akinaga and H. Shima, *Proc. IEEE* **98**, 2237 (2010); H. S. P. Wong, H. Y. Lee, S. M. Yu, Y. S. Chen, Y. Wu, P. S. Chen, B. Lee, F. T. Chen, and M. J. Tsai, *ibid.* **100**, 1951 (2012).
- ²W. Kim, S. Menzel, D. J. Wouters, Y. Guo, J. Robertson, B. Roesgen, R. Waser, and V. Rana, *Nanoscale* **8**, 17774 (2016); A. Calderoni, S. Sills, C. Cardon, E. Faraoni, and N. Ramaswamy, *Microelectron. Eng.* **147**, 145 (2015).
- ³S. H. Misha, N. Tamanna, J. Woo, S. Lee, J. Song, J. Park, S. Lim, J. Park, and H. Hwang, *ECS Solid State Lett.* **4**, P25 (2015).
- ⁴A. Prakash, D. Deleruyelle, J. Song, M. Bocquet, and H. Hwang, *App. Phys. Lett.* **106**, 233104 (2015).
- ⁵F. Miao, J. P. Strachan, J. J. Yang, M.-X. Zhang, I. Goldfarb, A. C. Torrezan, P. Eschbach, R. D. Kelley, G. Medeiros-Ribeiro, and R. S. Williams, *Adv. Mater.* **23**, 5633 (2011).
- ⁶U. Celano, L. Goux, R. Degraeve, A. Fantini, O. Richard, H. Bender, M. Jurczak, and W. Vandervorst, *Nano Lett.* **15**, 7970 (2015).
- ⁷A. Prakash, J. Park, J. Song, J. Woo, E. J. Cha, and H. Hwang, *IEEE Electron Device Lett.* **36**, 32 (2015).
- ⁸M. C. Wu, W. Y. Jang, C. H. Lin, and T. Y. Tseng, *Semicond. Sci. Technol.* **27**, 065010 (2012).
- ⁹S. Yu, Y. Wu, and H.-S. P. Wong, *Appl. Phys. Lett.* **98**, 103514 (2011).
- ¹⁰Y. Guo and J. Robertson, *Appl. Phys. Lett.* **105**, 223516 (2014).
- ¹¹M. J. Lee, C. B. Lee, D. Lee, S. R. Lee, M. Chang, J. H. Hur, Y. B. Kim, C. J. Kim, D. H. Seo, S. Seo, U. I. Chung, I. K. Yoo, and K. Kim, *Nat. Mater.* **10**, 625 (2011).
- ¹²K. Xiong, J. Robertson, and S. J. Clark, *J. Appl. Phys.* **99**, 044105 (2006); H. Li, Y. Guo, and J. Robertson, *Appl. Phys. Lett.* **104**, 192904 (2014).
- ¹³D. Ielmini, *IEEE Trans. Electron Devices* **58**, 4309 (2011).
- ¹⁴D. Ielmini, *Semicond. Sci. Technol.* **31**, 063002 (2016).
- ¹⁵P. Sun, S. Liu, L. Li, and M. Liu, *J. Semicond.* **35**, 104007 (2014).
- ¹⁶S. Kim, S. J. Kim, K. M. Kim, S. R. Lee, M. Chang, E. Cho, Y. B. Kim, C. J. Kim, U. I. Chung, and I. K. Yoo, *Sci. Rep.* **3**, 1680 (2013).
- ¹⁷Y. Guo and J. Robertson, *Appl. Phys. Lett.* **104**, 112906 (2014).
- ¹⁸Y. Guo and J. Robertson, *Microelectron. Eng.* **147**, 254 (2015).
- ¹⁹G. Shang, P. W. Peacock, and J. Robertson, *Appl. Phys. Lett.* **84**, 106 (2004).